Journal of Hydrology: Regional Studies 1 (2014) 107–128

Contents lists available at ScienceDirect

Journal of Hydrology: Regional Studies

journal homepage: www.elsevier.com/locate/ejrh

Impact of climate change on rainfall over Mumbai using Distribution-based Scaling of Global Climate Model projections

Arun Rana [a,*], Kean Foster [a,b], Thomas Bosshard [b], Jonas Olsson [b], Lars Bengtsson [a]

[a] Department of Water Resources Engineering, LTH, Lund University, Box No. 118, Lund 22100, Sweden
[b] Swedish Meteorological and Hydrological Institute, Norrköping 60176, Sweden

ARTICLE INFO

Article history:
Received 23 December 2013
Received in revised form 19 June 2014
Accepted 24 June 2014
Available online 2 August 2014

Keywords:
Distribution-based Scaling (DBS)
Global Climate Models (GCMs)
Impact analysis
Climate change
Mumbai

ABSTRACT

Study region: The study is carried out for Mumbai (18°58′30″ N, 72°49′33″ E).
Study focus: Future projections provided by general circulation models (GCMs) suggest the probability of occurrence of intense rainfall will change in the future. However, GCM data generally need to be downscaled and bias-corrected for impact studies. Although the domains covered by Regional Climate Models (RCMs) are increasing, statistical downscaling of GCM results is the main alternative in many regions. We applied a Distribution-based Scaling (DBS) procedure, with 1975–2004 as a reference period, for bias-correcting and downscaling daily rainfall data from nine global climate projections.
New hydrological insights for the region: The evaluation in the reference period showed that the scaled data are able to represent various key statistics. All GCMs were unable to accurately reproduce the southwest monsoon season. Using the transient DBS processed projection data, a comprehensive evaluation of key rainfall statistics was performed for three periods: near (2010–2040), intermediate (2041–2070) and distant future (2071–2099). There is an increase in the total accumulated annual rainfall, ranging from 300 to 500 mm in the ensemble. Also, a clear seasonal shift and delayed onset of the monsoon season evolves in the projections, with increasing and decreasing rainfall in September and June, respectively. A trend analysis using Student's *t* and Mann–Kendall tests was performed for 2010–2099. A significant positive trend was found for four of the GCM projections.

* Corresponding author. Tel.: +46 2224487; fax: +46 2224435.
E-mail addresses: arunranain@gmail.com, Arun.Rana@tvrl.lth.se (A. Rana).

http://dx.doi.org/10.1016/j.ejrh.2014.06.005

1. Introduction

Extreme weather events have severe consequences for human society. The impacts of the changing climate will likely be perceived most strongly through changes in intensity and frequency of climate extremes. Studies have found that human activities have contributed to an increase in concentrations of atmospheric greenhouse gases contributing to intensification of heavy rainfall events (Min et al., 2011). In the context of hydrology, the changing climate will likely accelerate the hydrological cycle on a global scale, and subsequently intensify the uneven spatial and temporal distribution of hydrological resources (Huntington, 2006; Trenberth, 1999). The intensity of extreme rainfall events is projected to increase under global warming in many parts of the world, even in the regions where mean rainfall decreases (e.g., Semenov and Bengtsson, 2002; Wilby and Wigley, 2002). Thus climate adaptation strategies for e.g. emergency planning, design of engineering structures, reservoir management, pollution control, or risk calculations rely on knowledge of the frequency of these extreme events (Kumke, 2001). Assessment of these extreme rainfall events is important in hydrological risk analysis and design of urban infrastructures. The increasing trend of rainfall extremes has quantifiable impacts on intensity duration frequency relations (Kao and Ganguly, 2011), and an increase in the intensity and/or frequency of extreme rainfall events may result in the flooding of urban areas (Ashley et al., 2005; Mailhot et al., 2007).

In India, rainfall variability is a central driver of the national economy as it is predominantly agricultural. A change in extreme events would have a large impact on the growing economy of India as most of the population live in urban areas. Several studies have addressed the issue of trends in rainfall in India since last century. Long-term southwest monsoon/annual rainfall trends over India as a whole were previously studied by Parthasarathy et al. (1993) and Rana et al. (2012), among others. Long term trends for the last 50 years indicate a significant decrease in the frequency of moderate-to-heavy rainfall events over most parts of India e.g., Dash et al. (2009) and Naidu et al. (1999). This is corroborated by a significant rise in the frequency and duration of monsoon breaks over India during recent decades (Ramesh Kumar et al., 2009; Turner and Hannachi, 2010), while the frequency of extreme rainfall events (100 mm/day) have increased in certain parts of the country (Goswami et al., 2006).

Future climate studies for India based on climate model simulations suggest that greenhouse driven global warming is likely to intensify the monsoon rainfall over a broad region encompassing South Asia (e.g., Lal et al., 2000; May, 2002, 2004, 2011; Meehl and Arblaster, 2003; Rupakumar et al., 2006). However, precise assessments of future changes in the regional monsoon rainfall have remained ambiguous due to wide variations among the model projections (e.g., Annamalai et al., 2007; Fan et al., 2010; Kripalani et al., 2007; Kumar et al., 2011; Sabade et al., 2011). The simulated rainfall response to global warming by climate models is actually accompanied by a weakening of the southwest monsoon (e.g., Kripalani et al., 2003; Krishnan et al., 2013; Sabade et al., 2011; Stowasser et al., 2009; Ueda et al., 2006). However, Rupakumar et al. (2006) have studied the effect of climate change in India by evaluating the present day simulation (1961–1990) of the PRECIS climate model and have reported an increase in extreme rainfall along the west coast and western parts of central India.

Several studies have investigated the vulnerability of Mumbai in the present and future climatic scenarios. Over the coming decades, the pressures of urbanisation may be aggravated by manmade climate change and increase in greenhouse gases. In the future, an increase in rainfall volume and/or intensity could increase the risk of severe flooding. Global Climate Models (GCMs) give a divergent picture of how precipitation will change in Northwest India over this century. The ensemble mean of the GCM projections assessed in IPCC (2007) suggests a small average increase in the summer precipitation (roughly 5% of 1990 levels by the 2090s), however this small average masks large positive and negative changes projected by individual models. Ranger et al. (2011) have presented a grim picture of Mumbai flooding and consequent economic losses during July 2005 floods and further analysed the situation in future scenarios. Further the authors have stressed the need to consider the implications of uncertainties in climate projections for adaptation planning in Mumbai. The authors have advocated the use of multiple projections from a range of available Global Climate Models and Regional Climate Models as a single scenario of future climate is by itself not adequate to inform robust adaptation decisions.

This present study, to the knowledge of the authors, is the only study being conducted to investigate the effects of climate change on the potential impacts of extreme rainfall in study area using data from several climate models. Many studies worldwide have described the possible impacts of climate change on urban drainage infrastructures and analysed the specific impacts on various urban areas, e.g. (Mailhot et al., 2007; Willems et al., 2012). These possible impacts could have serious implications for Mumbai, the economic hub of India.

In this study, we analyse the change of various precipitation statistics due to climate change for the city of Mumbai. General circulation models (GCMs) are currently the best way to model the complex climate processes that occur at the global scale, i.e. for studying possible future changes in climate mean, variability, and extremes (Huntingford et al., 2005). Climate change studies are essential in order to provide information for policy making and adaptation strategies (Stainforth et al., 2007). In most climate change studies, GCMs have been used to project future climatic variables. However, due to a limitation of GCMs to incorporate local topography (spatial and temporal scales), the direct use of their outputs in impact studies on the local scale of e.g. hydrological catchments is limited. To bridge the gaps between the climate model and local scales, downscaling is commonly used in practice. Dynamic downscaling and statistical downscaling are the most commonly used methods (Bergstrom, 2001; Fowler et al., 2007; Pinto et al., 2010; Schoof et al., 2009; Wilby et al., 1999). Dynamic downscaling by Regional Climate Models (RCMs) ensures consistency between climatological variables, however they are computationally expensive. Statistical downscaling models, on the other hand, are based on statistical relationships and hence require less computational time. Extensive research has been carried out with both approaches (e.g., Chen et al., 2012; Maraun et al., 2010; Teutschbein et al., 2011; Willems and Vrac, 2011).

Besides the scale issue, there is often a clear bias in the statistics of variables produced by GCMs such as rainfall and temperature (Kay et al., 2006; Kotlarski, 2005). Therefore hydrologically important variables need to be adjusted to obtain realistic time series for use in local impact studies (Graham et al., 2007). A conventional way to adjust future time series is referred to as bias correction (Lenderink, 2007) where correction factors are derived by comparing the GCM output with observed weather variables in the reference period, and then applied to GCM output for future climate. While bias-correction generally reproduces the variability described by different climatic conditions simulated by GCM projections, one disadvantage is the assumption of stationarity, i.e. that the correction factors do not change with time.

As indicated by Rana et al. (2012), the rainfall intensity and frequency for Mumbai is related to certain global climate indices such as the Indian Ocean Dipole, the El Niño-Southern Oscillation and the East Atlantic Pattern. These established connections between local rainfall and large-scale climate features suggest the possibility to statistically downscale GCM data directly to the local scale. The objective of this paper is to apply a statistical approach termed Distribution-based Scaling (DBS) technique, which has been tested and applied to RCM data, to scale GCM data. This includes the application of the DBS model to GCM projections for the area, an analysis of the scaling methodology and its applicability to GCM data, and finally assessment of the future impacts on the city of Mumbai due to climate change as projected by nine different GCM projections.

2. Study area, data and methods

2.1. Study area

The study is carried out for the city of Mumbai, (18°58′30″ N, 72°49′33″ E; formerly Bombay) the capital of Maharashtra state, located in the south-western part of India. Mumbai is located on the windward side of the Western Ghats of India and receives large rainfall amounts, owing to the orographic effect from strong westerly and south-westerly monsoon flows over the Arabian Sea. The average annual rainfall of Mumbai is 2142 mm with monsoon rainfall accounting for 96% of the total annual rainfall (Rana et al., 2012). During the monsoon, it usually rains uniformly over the city and severe flooding occurs in many parts. The duration of a rainfall event usually ranges from 30 min to

Table 1
List of CMIP5 GCMs used in present study.

Modelling centre	Model	Institution
BCC	BCC_CSM1.1	Beijing Climate Centre, China Meteorological Administration
CCCma	CanESM1.1	Canadian Centre for Climate Modelling and Analysis
INM	INM_CM4	Institute for Numerical Mathematics
IPSL	IPSL_CM5A_MR	Institut Pierre-Simon Laplace
NCAR	NCAR_CCSM4	National Centre for Atmospheric Research
NCC	NorESM1_M	Norwegian Climate Centre
CNRM-CERFACS	CERFACS_CNRM_CM5	Centre National de Recherches Meteorologiques/Centre Europeen de Recherche et Formation Avancees en Calcul Scientifique
MPI-M	MPI_ESM_LR	Max Planck Institute for Meteorology (MPI-M)
MOHC	HadGEM2_ES	Met Office Hadley Centre

120 min, however in some cases they can be as long as 3–4 h (Rana et al., 2013). Daily rainfall amounts of up to 250 mm are common during monsoon season (Rana et al., 2012).

2.2. Data

Observed daily rainfall data for the Colaba station (18°54′ N, 72°49′ E, 11 m.a.s.l) in Mumbai, covering the period 1975–2005, was obtained from the India Meteorological Department (IMD). The daily volume resolution is 0.1 mm and there is no missing daily data.

Further, daily rainfall data from nine GCM projections (see Table 1) was extracted from the CMIP5 database, provided by MOHC (Met Office Hadley Centre) (http://badc.nerc.ac.uk/home/) and we refer to the "WCRP Coupled Model Intercomparison Project" report and its references for details about the data (CLIVAR Exchanges; WCRP, 2011). All GCMs were driven by the Representative Concentration Pathway (RCP) 4.5. The RCP 4.5 is a stabilisation scenario where total radiative forcing is stabilised before 2100 by employment of a range of technologies and strategies for reducing greenhouse gas emissions (Van Vuuren et al., 2011). A large climate model ensemble of outputs driven by different models helps in quantifying the uncertainties in a comprehensive way and reduces errors associated with the GCMs.

Time series in the period 1975–2099 from the GCM grid cell covering Mumbai were extracted from each projection. We use the period 1975–2004 as the reference period, and the three periods 2010–2040, 2041–2070 and 2071–2099 as projection periods representing near, intermediate and far future, respectively.

2.3. Methods

2.3.1. Bias-correction

We have used the Distribution-based Scaling (DBS) Method (Yang et al., 2010) to downscale and bias-correct the GCM data for both historical and future projections. As for most bias-correction methods, it was assumed that simulations generated by GCMs for the control period cover the full range of climate processes and events that occur in the present climate, and is thus representative of present climate conditions up to a systematic and stationary bias. The DBS approach includes two steps. In the first step, the wet fraction (i.e. proportion of time steps with a non-zero precipitation) is adjusted to match the reference observations. A common feature of climate models is generation of "spurious drizzle", an excessive number of time steps with very low precipitation intensities (e.g. Maraun et al., 2010). The excessive drizzle can be quantified by comparing climate model output with gridded observations with the same spatial resolution. When comparing GCM output with point observations, as done here, an additional scale effect comes into play. As an area has a larger probability of rainfall than a point, the wet fraction should be larger for a time series from a GCM grid cell than from a station. The scale effect is, however, difficult to quantify and therefore we neglect it here and use the observed local wet fraction as a target for the GCM data. Thus simulated and observed daily rainfall was sorted in descending order and a cut-off value was defined as the threshold that reduced the percentage of wet

days in the GCM data to that of the observations. Days with rainfall amounts larger than the threshold value were considered as wet days and all other days as dry days (Yang et al., 2010).

In the second step of DBS, the remaining non-zero rainfall was transformed to match the observed cumulative probability distribution in the reference data by fitting gamma distributions to both observed and simulated daily rainfall. DBS applies a gamma distribution because of its documented ability to represent the typically asymmetrical and positively skewed distribution of daily rainfall intensities (Haylock et al., 2006). The density distribution of the two-parameter gamma distribution is expressed as:

$$f(x) = \frac{(x/\beta)^{\alpha-1}\exp(-x/\beta))}{\beta\Gamma(x)} \quad x, \alpha, \beta > 0 \tag{1}$$

where α is the shape parameter, β is the scale parameter and $\Gamma(x)$ is the gamma function. As the distribution of daily rainfall values is heavily skewed towards low intensities, distribution parameters estimated by e.g. maximum likelihood will be dominated by the most frequently occurring values and fail to accurately describe extremes. To capture the characteristics of normal rainfall as well as extremes, in DBS the rainfall distribution is divided into two partitions separated by the 95th percentile. Two sets of parameters – α, β representing non-extreme values and $\alpha 95$, $\beta 95$ representing extreme values – were estimated from observations and the GCM output for the reference period 1975–2004. These parameter sets were in turn used to bias-correct daily rainfall data from GCM outputs for the entire projection period up to 2099 using the following equations:

$$\begin{cases} P_{\mathrm{DBS}} = F^{-1}(\alpha_{\mathrm{Obs}}, \beta_{\mathrm{Obs}}, F(P, \alpha_{\mathrm{CTL}}, \beta_{\mathrm{CTL}})) & \text{if } P < 95\text{th percentile value} \\ P_{\mathrm{DBS}} = F^{-1}(\alpha_{\mathrm{Obs,95}}, \beta_{\mathrm{Obs,95}}, F(P, \alpha_{\mathrm{CTL,95}}, \beta_{\mathrm{CTL,95}})) & \text{if } P \geq 95\text{th percentile value} \end{cases} \tag{2}$$

where P denotes daily precipitation values of the GCMs and P_{DBS} stands for the DBS bias corrected daily precipitation data. The suffix Obs denotes parameters estimated from observations in the reference period and the suffix CTL denotes parameters estimated from the GCM output in the reference period. F represents the cumulative gamma probability distribution associated with the probability density function f (see equation 1). To take seasonal dependencies into account, the parameter sets were estimated for each season separately: pre-monsoon (March–May), Southwest monsoon (June–September), post-monsoon (October–November) and winter (December–February).

2.3.2. DBS evaluation and analysis of the climate change signal

Evaluation of DBS scaling procedure is done by comparing different climate statistics including accumulated rainfall, mean, standard deviation, coefficient of variation (CV), and percentage of annual rainfall for observed, raw GCM and bias-corrected GCM data. From the basic daily rainfall all the statistics were computed monthly for the southwest monsoon season and season-wise for the other seasons. Comparison between the simulations and observations are done on statistics for the whole evaluation period, i.e. not for individual days or years. A mean annual cycle curve, using a 31-day moving average, for the reference period was also plotted to evaluate the seasonal cycle more continuously. Rainfall extremes were studied by one-day, two-day, three-day and seven-day annual maxima, for all the years of a particular period individually. Annual maxima are then fitted using Lognormal and Gumbel distribution functions and the values for the 50 and 100-year return periods are determined. Also, percentage frequency of different rain intensities in observed, raw GCM and bias-corrected GCM data were calculated.

The analysis of the climate change signal is done for all the nine GCM projections and their ensemble mean, and for the periods 2010–2040, 2041–2070, 2071–2099 and 2010–2099. The extreme value statistics in future period were subjected to Mann–Kendall and Student's t tests (linear regression) for long-term trend analysis for the whole transient period (2010–2099). The linear regression method is widely used to determine long-term trends seasonally, annually, and for daily maximum rainfall e.g. Gadgil and Dhorde (2005), among many others. The non-parametric Mann–Kendall test is used here as a significance test.

3. Results and discussion

We have divided the results section into three parts where we present the evaluation of DBS scaling procedure in the reference period in Section 3.1, followed by the analysis of the climate projections for the near future (2010–2040), intermediate future (2041–2070) and distant future (2071–2099) (Section 3.2), and Section 3.3 finally deals with trend analysis for the entire future period (2010–2099) for detecting any long-term trends in the climate projections.

3.1. Evaluation of the DBS methodology for rainfall during the reference period (1975–2004)

The evaluation statistics, including accumulated rainfall, mean, standard deviation, coefficient of variation and percentage contribution to annual rainfall for seasonal, monsoon and annual data period, are presented in Table 2. For brevity, we show the results of all statistical comparison with the observed data only for projections NCAR_CCSM4 and the NorESM1_M, as these models give the closest representation of observed data in terms of accumulated precipitation. All the models were under estimating the total accumulated precipitation as compared to observations (Appendix 1).

It can be observed from Table 2 that there is a marked improvement in the reproduction of the climate statistics for both models after post-processing by DBS in comparison to the raw model. Accumulated rainfall is substantially improved for the entire period from 47,914 mm to 58,001 mm and from 31,286 mm to 60,071 mm for the NCAR_CCSM4 and NorESM1_M projection, respectively, compared to the observed 58,104 mm of rainfall. The same can be said for other annual statistics. Notably, the DBS procedure is able to reproduce the pattern of rainfall during different seasons. The monsoon season, which accounts for nearly 96% of rainfall (Rana et al., 2012), is well represented in the scaled data. The original values 85.1% and 85% in the raw NCAR_CCSM4 and NorESM1_M projections, respectively, after DBS application increase to 94.3% and 95.1%, as compared to 95.8% in the observations. It can be observed in Table 2 that there is slight overestimation of rainfall in the post-monsoon season (especially for September), while rainfall in June is underestimated, indicating a delayed onset of the Monsoon season in the GCMs (see also Fig. 1). The DBS application is not able to correct this late onset of the monsoon in the GCMs (Fig. 1), and the case may be the same when we are analysing future projections. This can also be observed for individual months during the monsoon season, as a slight correctional shift in the amount of rainfall received compared to observed data.

Extreme value statistics are represented in Table 3 and Fig. 2 for 1, 2, 3 and 7 consecutive days. In the case of raw GCM data the extremes are below the observed values (Fig. 2), which is to be expected considering the differing spatial scales of a GCM compared to a precipitation station. It can be observed from the table that the mean (153 mm) and standard deviation (42.2 mm) of extreme events for all the observed data (1-day maximum) are well represented in the DBS-corrected GCM data, being 154 mm and 45.8 mm, respectively, for the NCAR_CCSM4 projection and 139.9 mm and 51.2 mm, respectively, for the NorESM1_M projection. The same can be observed for 2, 3 and 7-day maximum values where there is marked improvement in the statistics after the scaling procedure.

Observed 1-day Lognormal values for the 50 (284 mm) and 100 (309.6 mm) year return periods are well represented in the scaled data, being 282 mm and 307 mm for NCAR_CCSM4 and 285 mm and 31 6 mm for NorESM1_M, respectively. Similarly, the 1-day Gumbel distribution values for the 50 (263 mm) and 100 (286 mm) year return periods are well represented in the scaled data, being 272 mm and 297 mm for NCAR_CCSM4 and 272 mm and 300 mm for NorESM1_M, respectively. Lognormal distribution is a continuous probability distribution whose logarithm is normally distributed whereas Gumbel come from distributions that are not bounded above but do have a full set of finite moments. Thus the two provides different facets of data maximum. In our results, there is a systematical difference between the values obtained from Lognormal and Gumbel distribution fitting wherein Lognormal values are always a bit higher than Gumbel in the observed, raw and bias-corrected datasets.

The rainfall intensity histogram for the entire reference period is presented in Fig. 3. The raw GCM data show a lower number of dry days (i.e. days with no rainfall), they generally overestimate the

Table 2
Climate statistics of observed data, raw and bias-corrected GCM data.

Month/season			Annual	June	July	August	September	Pre-monsoon	Southwest monsoon	Post monsoon	Winter
Observed		Rainfall accumulated (mm)	58,104.0	7807.0	20,547.0	16,380.0	8826.0	30.0	53,560.0	4336.0	90.0
		Mean (mm)	1936.8	260.2	684.9	546.0	294.2	1.0	1785.3	144.5	3.0
		Standard deviation (mm)	369.9	210.9	217.4	251.5	150.2	2.9	334.4	150.6	5.1
		CV (%)	19.1	81.0	31.7	46.1	51.0	285.3	18.7	104.2	170.9
		Percentage to annual (%)	100.0	13.4	35.4	28.2	15.2	0.1	92.2	7.5	0.2
NCAR_CCSM4	Raw data	Rainfall accumulated (mm)	47,914.0	5290.0	13,795.0	13,365.0	8334.0	835.0	40,784.0	4608.0	1530.0
		Mean (mm)	1597.1	176.3	459.8	445.5	277.8	27.8	1359.5	153.6	51.0
		Standard deviation (mm)	254.0	139.6	150.3	150.0	118.6	26.3	254.5	58.8	37.1
		CV (%)	15.9	79.2	32.7	33.7	42.7	94.3	18.7	38.3	72.8
		Percentage to annual (%)	100.0	11.0	28.8	27.9	17.4	1.7	85.1	9.6	3.2
	DBS corrected	Rainfall accumulated (mm)	58,001.0	6833.0	19,066.0	18,159.0	10,664.0	500.0	54,722.0	1841.0	827.0
		Mean (mm)	1933.4	227.8	635.5	605.3	355.5	16.7	1824.1	61.4	27.6
		Standard deviation (mm)	428.6	225.7	256.1	248.3	192.6	44.9	425.6	62.1	31.7
		CV (%)	22.2	99.1	40.3	41.0	54.2	269.5	23.3	101.3	115.1
		Percentage to annual (%)	100.0	11.8	32.9	31.3	18.4	0.9	94.3	3.2	1.4
NorESM1_M	Raw data	Rainfall accumulated (mm)	31,286.0	1763.0	7389.0	10,970.0	6460.0	330.0	26,582.0	3143.0	1091.0
		Mean (mm)	1042.9	58.8	246.3	365.7	215.3	11.0	886.1	104.8	36.4
		Standard deviation (mm)	288.7	58.4	84.8	165.3	94.0	9.9	256.2	63.6	24.7
		CV (%)	27.7	99.4	34.4	45.2	43.7	90.4	28.9	60.7	68.0
		Percentage to annual (%)	100.0	5.6	23.6	35.1	20.6	1.1	85.0	10.0	3.5
	DBS corrected	Rainfall accumulated (mm)	60,071.0	3171.0	15,558.0	24,862.0	13,522.0	439.0	57,113.0	1618.0	794.0
		Mean (mm)	2002.4	105.7	518.6	828.7	450.7	14.6	1903.8	53.9	26.5
		Standard deviation (mm)	687.0	140.7	216.4	433.5	231.5	29.6	657.8	64.6	33.4
		CV (%)	34.3	133.1	41.7	52.3	51.4	202.3	34.6	119.8	126.2
		Percentage to annual (%)	100.0	5.3	25.9	41.4	22.5	0.7	95.1	2.7	1.3

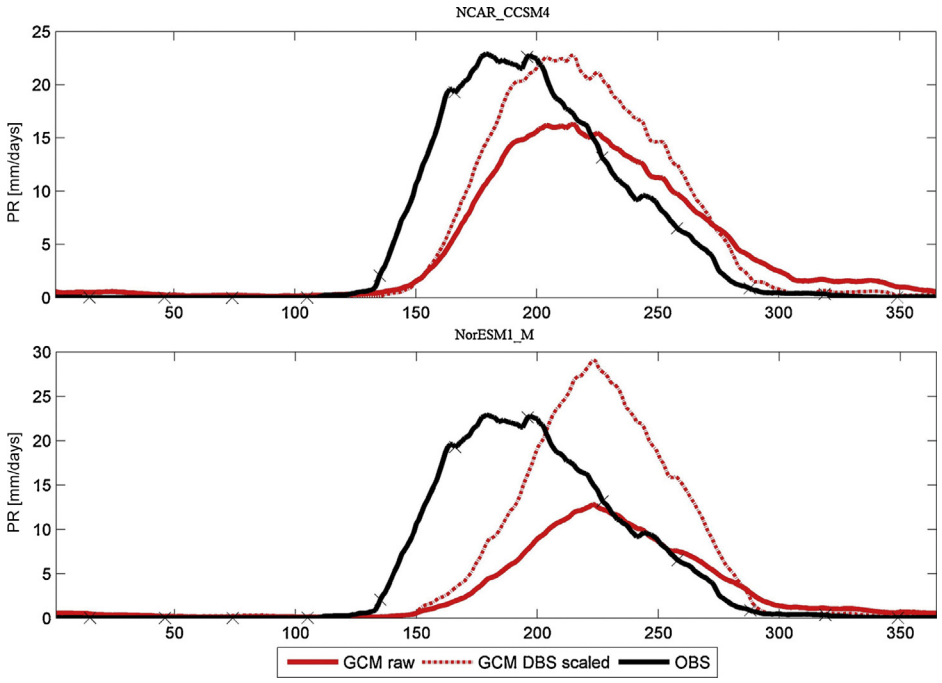

Fig. 1. Mean annual rainfall cycle over the 30 year reference period (1975–2004) using a 31 day moving average of the observed, raw and bias-corrected GCM data.

Table 3
Extreme value statistics of observed, raw and bias-corrected GCM annual maxima with Lognormal and Gumbel distributions.

Distribution				Lognormal		Gumbel	
Model	Time step	Mean (mm)	Standard deviation (mm)	T50 (mm)	T100 (mm)	T50 (mm)	T100 (mm)
Observed	Daily Max	153.6	42.2	284.0	309.6	263.0	286.0
	2 day Max	244.6	66.4	451.6	492.4	416.6	452.7
	3 day Max	308.5	73.2	573.8	625.5	498.3	538.1
	7 day Max	478.1	106.9	893.0	973.5	755.3	813.5
Raw NCAR_CCSM4	Daily Max	96.8	36.4	201.5	224.3	191.1	211.0
	2 day Max	149.6	52.8	309.4	343.9	286.5	315.2
	3 day Max	183.5	64.1	365.8	404.4	349.5	384.4
	7 day Max	268.7	78.2	491.3	535.6	471.5	514.0
DBS corrected NCAR_CCSM4	Daily Max	154.2	45.8	282.0	307.4	272.8	297.7
	2 day Max	244.8	74.3	475.4	523.0	437.5	478.0
	3 day Max	299.7	96.5	579.8	637.8	549.9	602.4
	7 day Max	426.3	128.3	808.3	886.0	759.0	828.9
Raw NorESM1_M	Daily Max	53.2	20.7	106.3	117.6	106.8	118.1
	2 day Max	88.3	35.0	174.5	192.7	179.1	198.1
	3 day Max	110.7	44.0	211.6	232.6	224.7	248.7
	7 day Max	174.1	65.0	320.1	349.7	342.6	378.0
DBS corrected NorESM1_M	Daily Max	139.9	51.2	285.0	316.1	272.7	300.6
	2 day Max	232.8	90.0	480.7	534.5	466.1	515.1
	3 day Max	287.9	115.7	581.2	644.2	587.8	650.7
	7 day Max	435.5	177.4	864.2	955.6	895.4	992.0

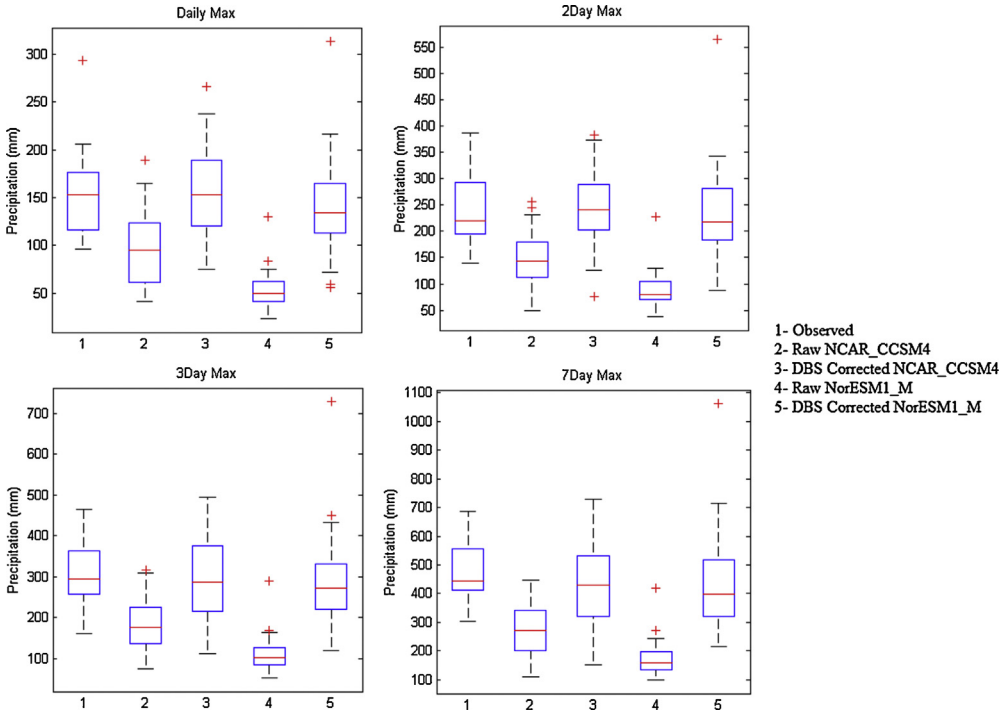

Fig. 2. Box plots of extreme value statistics for the observed, raw and bias-corrected GCM data for 1, 2, 3 and 7-day maximum values.

frequency in the intensity interval of 0–20 mm, and underestimate the frequency of intensities above 40 mm. This is an expected consequence of the difference in spatial scales between the data sets, but may also reflect GCM bias. In contrast, the rainfall intensity histogram of the DBS corrected model data closely follows that of the observed data for both models. High intensity/frequency events (more than 80 mm/day) in the scaled data are apparent and are in line with the observed data.

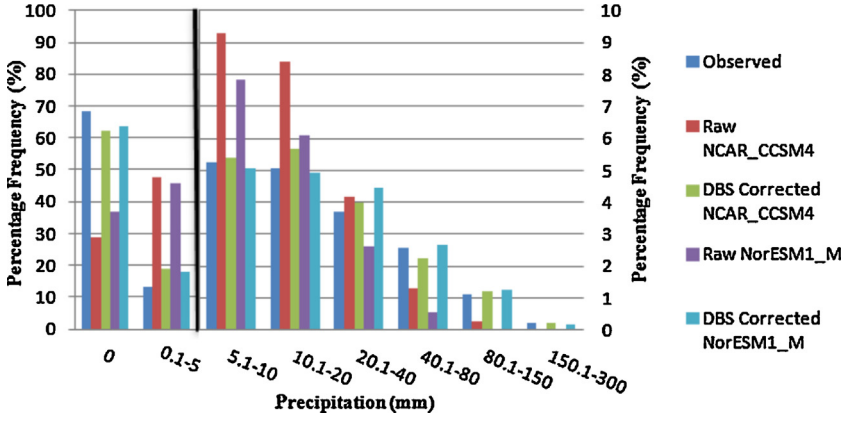

Fig. 3. Frequency of rainfall events in the observed, raw and bias-corrected GCM data. (*Note*: The right axis is applicable for the graph to the right of the black vertical line).

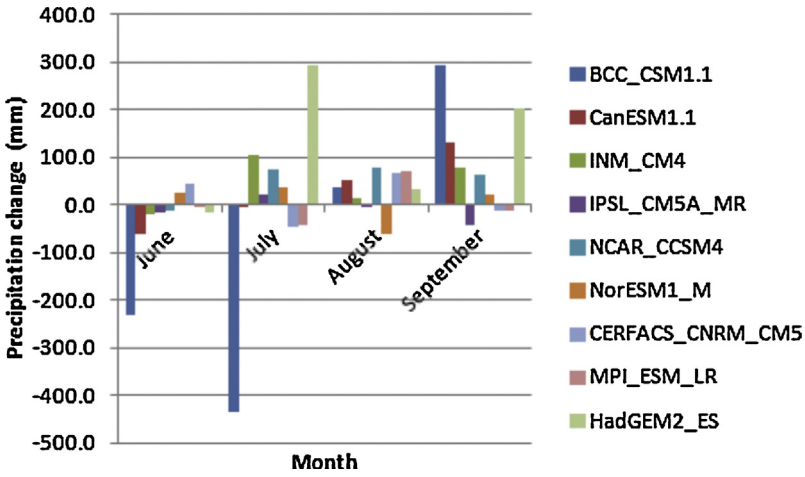

Fig. 4. Absolute change of precipitation in near future DBS corrected data (2010–2040) over the monsoon months as compared to baseline DBS corrected data (1975–2004).

3.2. Evaluation for climate projections for the near future (2010–2040), intermediate future (2041–2070) and distant future (2071–2099)

3.2.1. The near future projection

In Table 4, climate statistics for near future projections are presented for annual, pre-monsoon, monsoon, post monsoon and winter seasons. It should be noted that most of the projections are indicating an increase in mean annual rainfall as compared to the observed baseline mean of 1936 mm. The ensemble mean suggests an increase of around 140 mm for the city with a range – between 18 mm decrease and 500 mm increase for the different projections. Similar changes can be observed in the monsoon season for all the projections. There are relatively small changes in CV which is 22.9% and 27.2% for the annual and monsoon season as compared to 19.1% and 18.7% for the observed baseline projection suggesting slightly higher variability in the near future.

Fig. 4 represents the absolute change of the mean monthly precipitation between the DBS corrected projections as compared to the bias-corrected projections in the reference period during the monsoon season. It can be observed that all projections project a lower rainfall contribution during June, approximately the same during July and a higher rainfall contribution in the months of August and September. In comparison, the observed values are relatively high in July–August and low in June and September, which can be attributed to a bias in the raw GCM data as was indicated in Fig. 1. The overall percentage contribution to the monsoon season is relatively conserved as compared with the reference data with an increase in the total rainfall received.

3.2.2. The intermediate future projection

All the projections indicate an increase in mean annual rainfall as compared to the observed mean value of 1936 mm. The ensemble mean suggests an increase of around 300 mm in rainfall for the city and the same can be observed in the monsoon season for all the projections. There is a relatively larger change (when compared to the near future projections) in CV which is 30.7% and 31.3% for the annual and the monsoon season, respectively, as compared to 19.1% and 18.7% for the reference period suggesting a higher variability than that observed in near future projections. The absolute change of the mean monthly precipitation for the monsoon season is presented in Fig. 5. It can be pointed out that all the models are suggesting a lower rainfall contribution during June, approximately the same during July and a higher rainfall contribution in the months of August and September, similar to what

Table 4
Climate statistics for near future DBS corrected GCM projections (2010–2040). The values in brackets represent the absolute change in the DBS corrected GCM data when comparing the near future and the reference period i.e. DBS-GCM (2010–40) – DBS-GCM (1979–2004).

Month/season		Annual	Pre-monsoon	Southwest monsoon	Post monsoon	Winter
BCC_CSM1.1	Mean (mm)	2024.5 (0.7)	20.5 (5.1)	1592.0 (−338.0)	391.2 (343.4)	2092.1 (2064.7)
	Standard Deviation (mm)	8.8 (−458.7)	34.2 (−3.9)	512.6 (58.1)	265.3 (220.4)	716.7 (679.6)
	CV (%)	0.4 (−22.7)	166.9 (−81.0)	32.2 (8.6)	67.8 (−26.1)	34.3 (−101.2)
CanESM1.1	Mean (mm)	2040.5 (124.7)	20.5 (3.9)	1927.3 (113.8)	69.3 (15.4)	34.7 (6.0)
	Standard Deviation (mm)	566.7 (−141.8)	34.2 (0.6)	551.2 (−141.7)	68.3 (3.9)	76.9 (36.0)
	CV (%)	27.8 (−9.2)	166.9 (−35.2)	28.6 (−9.6)	98.5 (−21.0)	221.8 (79.1)
INM_CM4	Mean (mm)	2388.2 (209.5)	20.5 (3.5)	2224.1 (174.8)	52.3 (−10.0)	72.6 (26.2)
	Standard Deviation (mm)	706.3 (73.5)	34.2 (−15.5)	664.9 (59.3)	66.9 (−19.5)	68.4 (20.5)
	CV (%)	29.6 (0.5)	166.9 (−125.5)	29.9 (0.3)	127.9 (−10.7)	94.3 (−8.9)
IPSL_CM5A_MR	Mean (mm)	2347.5 (−18.6)	20.5 (7.8)	2220.6 (−38.2)	77.6 (32.4)	28.6 (−17.6)
	Standard Deviation (mm)	610.8 (−98.4)	34.2 (7.1)	625.0 (−60.9)	96.2 (35.2)	47.9 (−4.3)
	CV (%)	26.0 (−4.0)	166.9 (−47.1)	28.1 (−2.2)	124.0 (−11.1)	167.5 (54.4)
NCAR_CCSM4	Mean (mm)	2132.0 (198.7)	20.5 (3.8)	2023.9 (199.8)	65.6 (4.2)	26.1 (−1.4)
	Standard Deviation (mm)	407.1 (−21.5)	34.2 (−10.7)	406.3 (−19.3)	68.2 (6.1)	22.3 (−9.5)
	CV (%)	19.1 (−3.1)	166.9 (−102.5)	20.1 (−3.3)	104.0 (2.7)	85.1 (−29.9)
NorESM1_M	Mean (mm)	2016.3 (13.9)	20.5 (5.8)	1923.7 (20.0)	52.6 (−1.4)	29.1 (2.6)
	Standard Deviation (mm)	585.7 (−101.3)	34.2 (4.6)	587.9 (−69.9)	62.6 (−2.0)	37.0 (3.6)
	CV (%)	29.0 (−5.3)	166.9 (−35.3)	30.6 (−4.0)	119.1 (−0.7)	127.2 (1.0)
CERFACS_CNRM_CM5	Mean (mm)	2074.6 (123.5)	20.5 (4.4)	1921.1 (55.3)	71.1 (8.2)	16.5 (12.5)
	Standard Deviation (mm)	450.1 (0.5)	34.2 (−3.0)	435.5 (−3.0)	89.6 (−10.6)	35.2 (25.8)
	CV (%)	21.7 (−1.3)	166.9 (−64.7)	22.7 (−0.8)	126.1 (−33.4)	214.0 (−24.0)
MPI_ESM_LR	Mean (mm)	2243.5 (34.2)	20.5 (7.9)	2141.8 (11.4)	83.2 (27.0)	8.5 (0.8)
	Standard Deviation (mm)	506.5 (15.2)	34.2 (−1.9)	487.1 (−10.3)	79.4 (25.0)	12.6 (−7.9)
	CV (%)	22.6 (0.3)	166.9 (−121.1)	22.7 (−0.6)	95.5 (−1.5)	148.7 (−118.7)
HadGEM2_ES	Mean (mm)	2547.1 (491.4)	20.5 (5.2)	2479.5 (512.3)	41.0 (−18.7)	8.4 (−2.3)
	Standard Deviation (mm)	772.4 (166.7)	34.2 (−0.2)	741.9 (143.5)	68.7 (1.4)	21.2 (2.6)
	CV (%)	30.3 (0.8)	166.9 (−58.0)	29.9 (−0.5)	167.6 (54.9)	251.9 (77.7)
Average	Mean (mm)	2201.6 (130.9)	20.5 (5.3)	2050.4 (79.0)	100.4 (44.5)	257.4 (232.4)
	Standard Deviation (mm)	512.7 (−62.9)	34.2 (−2.6)	556.9 (−4.9)	96.1 (28.9)	115.3 (82.9)
	CV (%)	22.9 (−4.9)	166.9 (−74.5)	27.2 (−1.3)	114.5 (−5.2)	149.4 (−7.8)

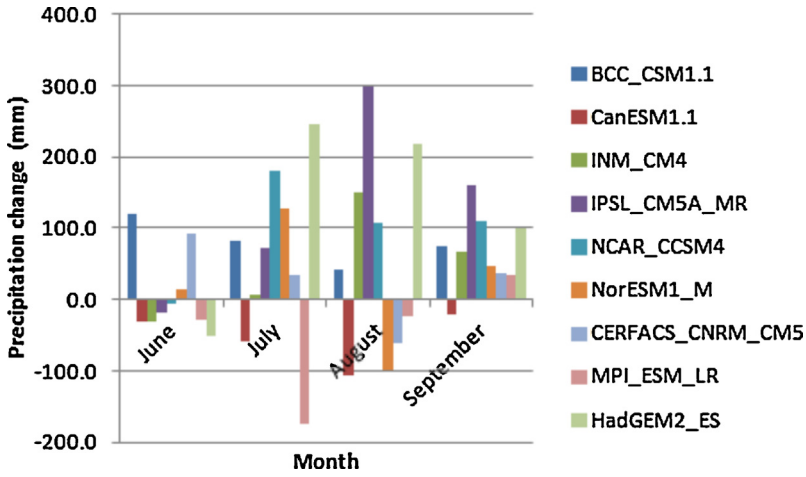

Fig. 5. Absolute change of precipitation in intermediate future DBS corrected data (2041–2070) over the monsoon months as compared to baseline DBS corrected data (1975–2004).

was observed in the near future projection. The overall percentage contribution to monsoon season is similar to that in the reference period.

3.2.3. The distant future projection

All the models are indicating an increase in mean annual rainfall as compared to the observed reference mean of 1936 mm, and the average of all the models is 2350 mm. There is a relatively large change when compared to the near future projections and a relatively small change when compared to the intermediate projections in terms of CV, which is reported as 25.6% and 27.2%, respectively, for the annual and monsoon season. This is close to the reference period, suggesting low variability. Concerning monthly rainfall, Fig. 6 suggests a lower rainfall contribution during June, approximately the same during July and a higher rainfall contribution in the months of August and September as was observed in the reference data (Fig. 1), near future and intermediate future projections. The overall percentage contribution to the monsoon season is relatively well represented and in line with the

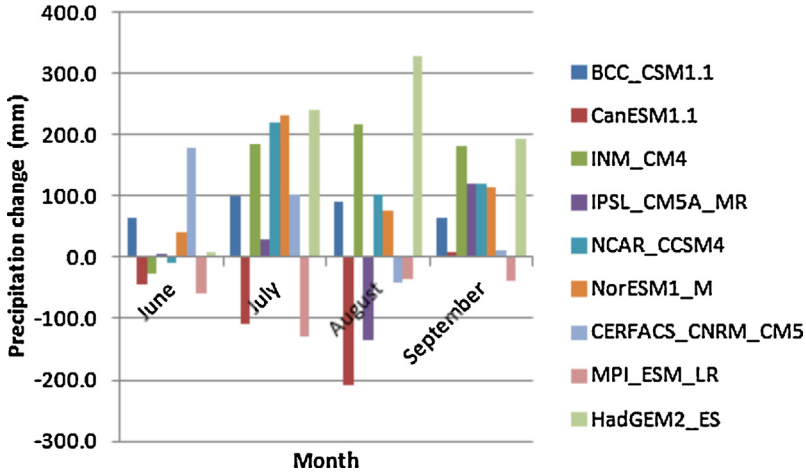

Fig. 6. Absolute change of precipitation in distant future DBS corrected data (2071–2100) over the monsoon months as compared to baseline DBS corrected data (1975–2004).

reference monsoon precipitation data. There is also a relative increase in the amount of rainfall received during the monsoon months for all the projection runs.

3.3. Trends in the long term/transient (2010–2099) climate projections and evaluation of extreme events for all projections

Fig. 7 represents the trends in daily maximum precipitation, as estimated by the different projections, across the whole time scale considered for this study. Different data periods are marked with different colours and trends lines are depicted for each near, intermediate, distant and transient periods. It can be observed from the figure that most of the models show a positive trend except CanESM1.1, CERFACS_CNRM_CM5 and MPI_ESM_LR. A trend analysis for the entire future period is presented in Table 5 and extreme values are depicted in Fig. 8 (absolute change in different models with respect to baseline scenario). It can be observed from Table 5 that four out of the projections are suggesting a significant positive trend in the extreme rainfall. Three out of the projections show a decreasing trend but these are not significant at the 0.05 level. It should be noted that six of the projections indicate a positive trend in maximum daily rainfall and that the average of all the projections point towards a positive trend in daily events in both the Student's *t*-test and Mann–Kendall analyses.

Fig. 8 shows the absolute change in maximum rainfall with respect to baseline scenario, in bias-corrected datasets, for the 50-year return period as 100 mm and 60 mm (Lognormal and Gumbel distributions respectively) and 200 mm and 100 mm for 100-year return period (Lognormal and Gumbel distributions respectively). The maxima (T50 and T100) range from 210 to 450 mm for different models in transient future scenario. This is relatively higher than the observed values. The difference between Lognormal and Gumbel distribution values can be explained by the systematic difference in the methods itself and it was observed in reference period as well. As per the future scenarios, both the distributions are predicting higher values than observed reference period values except in three models. The range of increase is in range of 50–100 mm. The average maximum values are increasing as we move from near to intermediate and decreasing from intermediate to distant future scenario for both T50 and T100 and for Lognormal and Gumbel distribution. Effectively there is always an increase in maximum values for both distribution and for both return periods for the transient future scenario indicating an increase in extreme precipitation.

It appears that maximum values are following a 30-year cycle of first increase then stabilising and increasing again in distant future scenarios. Similar results were obtained by Rana et al. (2012) where the precipitation maximum were following the climatic indices cycle. The magnitude of the change as well as the range of variability differs between projections, which is attributed to the different models used in the study.

4. Discussion

Overall, the results show that the intensity of rainfall, which is already relatively high considering the design standard of 25 mm/h for Mumbai (Gupta, 2007), is projected to increase in the future. The average increase in maximum rainfall is about ~15–20% in each 30-year time slice and ~30–45% in the 90-year transient period. This can also be inferred from Fig. 8, where changes in maxima corresponding to 50- and 100-year return periods are shown with respect to baseline scenario. These results imply an increased hydrological risk for the city of Mumbai, as also pointed out by Rana et al. (2013) in their development of IDF curves and risk assessment based on historical data. The projections presented here could provide valuable information for risk management and climate adaptation planning in Mumbai. They can also be used to estimate relative change in the amount of precipitation received in monsoon season as compared with other seasons, which may be important for water resources management.

Results from the present study can be compared in accordance to findings from other studies where most of them indicated towards intensification of the monsoon rainfall over a broad region encompassing South Asia (e.g., Lal et al., 2000; May, 2002, 2004, 2011; Meehl and Arblaster, 2003;

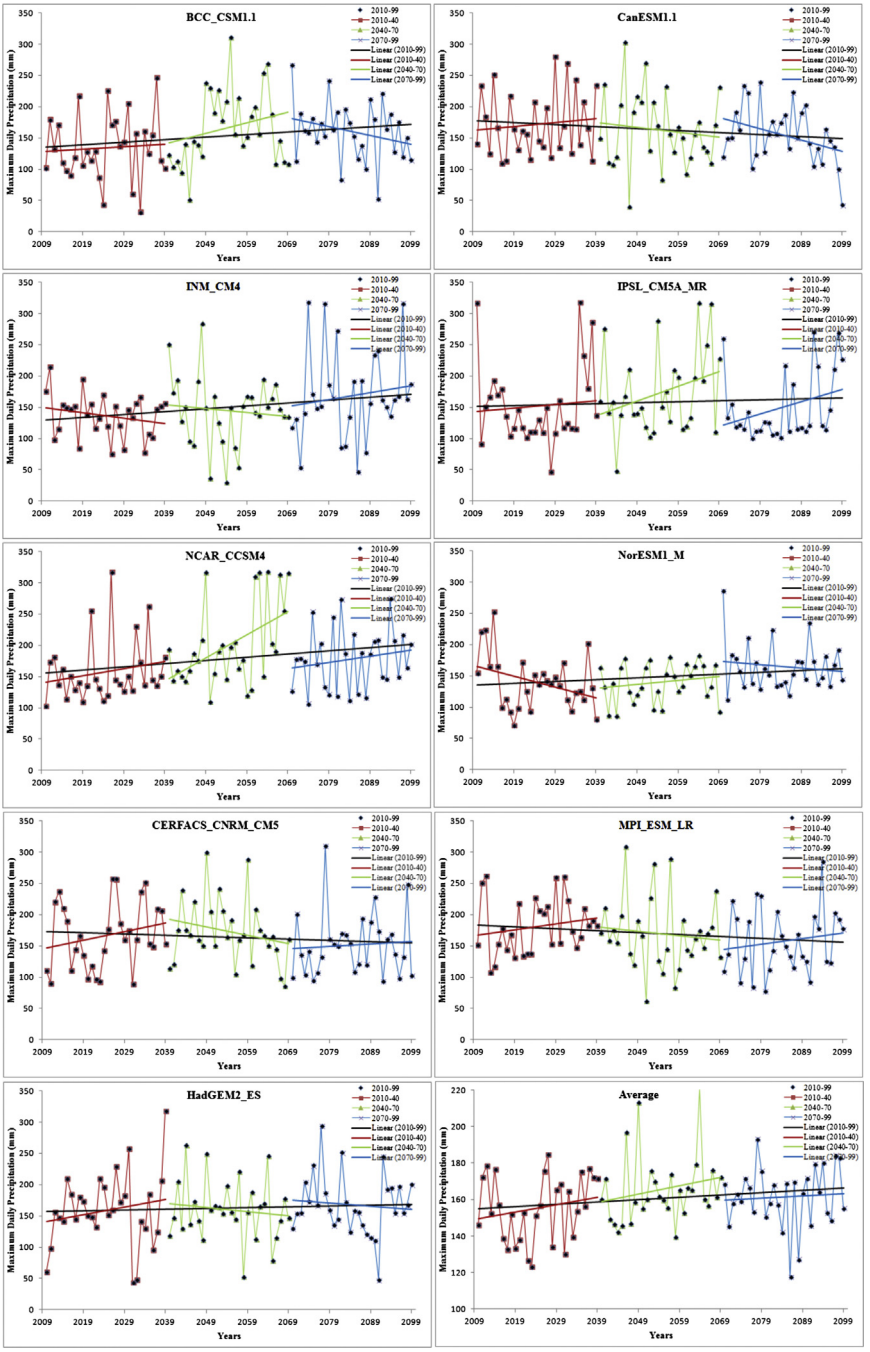

Fig. 7. Trends in the daily maximum rainfall in the climate projections; near future (2010–2040), intermediate future (2041–70), distant future (2071–99) and transient future (2010–99).

Table 5
Extreme event statistics and trend analysis for the period 2010–2099 using both a Student's *t* test and a Mann–Kendall test (figures in bold are significant at the 0.05 level).

Model	Mean (mm)	Standard deviation (mm)	Regression slope	Intercept (mm)	Correlation coefficient	Student's *t* test (*t*)	Mann–Kendall test (*Z*)
BCC_CSM1.1	153.867	53.195	0.406	135.409	0.198	**1.907**	**1.984**
CanESM1.1	163.211	51.067	−0.327	178.082	−0.166	−1.591	−1.283
INM_CM4	149.768	56.168	0.463	128.681	0.214	**2.07**	**1.886**
IPSL_CM5A_MR	158.282	61.288	0.16	151.024	0.068	0.01	0.342
NCAR_CCSM4	178.532	56.723	0.519	154.94	0.237	**2.306**	**2.92**
NorESM1_M	148.256	38.559	0.299	134.673	0.201	**1.937**	**2.426**
CERFACS_CNRM_CM5	163.538	50.924	−0.2	172.627	−0.102	−0.966	−1.193
MPI_ESM_LR	169.39	50.88	−0.311	183.548	−0.159	−1.518	−1.464
HadGEM2_ES	162.224	50.615	0.128	156.411	0.066	0.01	0.6
Average	160.7853	52.15767	0.126333	155.0439	0.061889	0.462778	0.690889

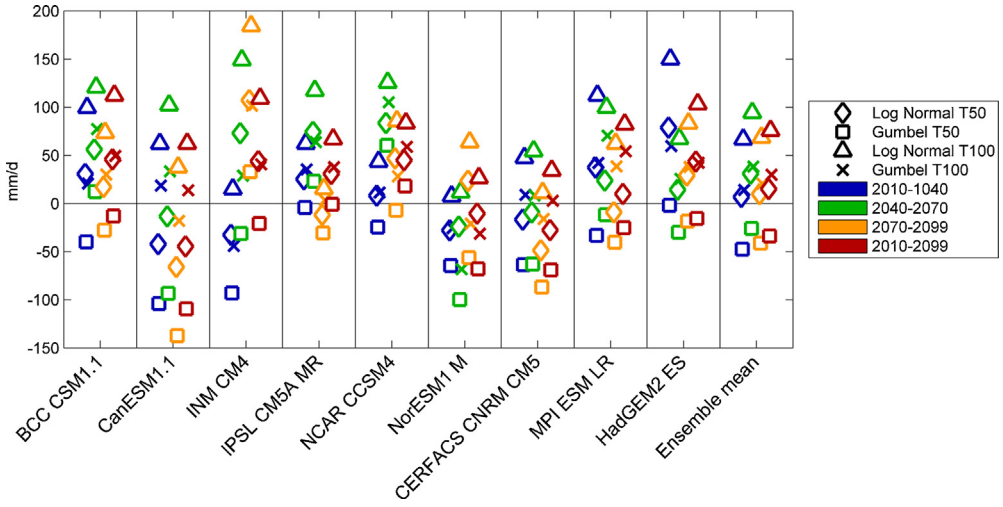

Fig. 8. Extreme value statistics for the 50 year and 100 year return periods for the observations, near future (2010–2040), intermediate future (2041–70), distant future (2071–99) and long-term future (2010–99) projections.

Rupakumar et al., 2006). Though these studies were on a broader scale, they were indicating towards intensification of rainfall in areas the show the same monsoon phenomena which is dominant in rainfall for Mumbai. Ranger et al. (2011) has also indicated an intensification of rainfall in the study area using a single model output and estimated the socio-economic consequences of it.

The results of the present study, using scaling techniques to bias-correct GCM projections to the local scale, should be seen as potentially useful for impact studies. In urban areas, it is very important to study the effects of extreme rainfall events and increases in net rainfall and rainfall–runoff relationships. Changes in the physical characteristics of urban areas change the runoff response of the area along with natural forces. Thus, it is necessary to evaluate the effect of changes in rainfall and human interference on the natural drainage patterns of the urban area. Infrastructural planning of urban areas should require careful attention to urban drainage characteristics. This study could be useful for adaptation studies in future for the study area. The projections presented here could provide valuable information for risk management and climate adaptation planning in Mumbai. They can also be used to find out the intensity of storms and relative change in the amount of precipitation received in monsoon season over the period of time, i.e. future scenario period, and can serve as important criteria for the design of drainage systems and other infrastructure facilities.

Nevertheless, there are considerable sources of uncertainties in the results, related mainly to the climate projections ability of describing the probability of occurrence of extreme events. Further, due to the nature of extreme events, there is only limited data available and the inherent natural or internal variability add uncertainty to the analysis of results. The uncertainties can also be attributed to GCM bias (e.g. Fig. 1). Downscaling and bias-correction methodologies like DBS can be used in climate change studies for regions with data from only single stations and without commonly available regional projections. Using an ensemble of climate projections, as in this study, can provide an estimate of the uncertainty related to model structures and internal variability. The choice of statistical downscaling and bias-correction method, however, also adds up to the total uncertainty in the final result and it may be considered using different methods. Improvements are still required in climate model post-processing methodologies to deal with such substantial biases, e.g. related to inaccurate timing and location of stationary synoptic-scale rainfall fields like the monsoon. There are developments in studying the impact of climate change at the regional scale but options need

to be explored further for reduction of uncertainties associated with GCM data and scaling procedures.

5. Concluding remarks

Main findings of the present study are outlined below:

1. Comparison of point observations in Mumbai with raw GCM projections in the reference period shows that GCMs underestimates the mean and extreme precipitation in the study area.
2. After the application of DBS, the agreement in the reference period improves considerably and the climatic characteristics in the observed reference data are well reproduced. Thus, DBS has proved capable of improving the representation of local rainfall statistics.
3. Results have indicated an increased amount of precipitation received in the study area in all future climatic projections. The increase in the amount of precipitation ranges from 20% to 40% in various projections.
4. The same can be said about extreme events of rainfall as tested for the 50 and 100-year return periods using Lognormal and Gumbel distribution functions. The increase in the extreme events ranges from 0% to 40% with two projections indicating a slight decrease.
5. Six out of nine projections show a positive trend of rainfall extremes in the period 2010–2099, including four showing a significant positive trend at the 0.05 level.

This study has provided a more clear picture the future changes of rainfall in the Mumbai area than what has been previously available. Further knowledge about the expected future changes are to be provided by the on-going work with regional climate projections for India within the Coordinated Regional Downscaling Experiment (CORDEX; Giorgi et al., 2009). As discussed above, the changes may have negative hydrological impacts such as an increased flood risk (see also e.g. Ranger et al., 2011). There is a need to incorporate detailed hydrological impact modelling studies to better assess the future impacts on the study area. This conceivably includes climate projections by both hydraulic models of the drainage systems and by hydrological models for the Mumbai region.

Conflict of interest

Authors declare that there is no conflict of interest.

Acknowledgments

The authors would like to acknowledge the World Climate Research Programme's Working Group on Coupled Modelling, which is responsible for CMIP, and we thank the climate modelling groups (listed in Table 1) for producing and making available their model outputs. For CMIP, the U.S. Department of Energy's Program for Climate Model Diagnosis and Intercomparison provides coordinating support and leads development of software infrastructure in partnership with the Global Organization for Earth System Science Portals. Funding from the Swedish Research Council Formas (grant no. 2010-121) and the Swedish International Development Agency (SIDA) (grant no. AKT-2012-022) is gratefully acknowledged.

Appendix 1.

Month/season			Annual	June	July	August	September	Pre-monsoon	Southwest monsoon	Post monsoon	Winter
Observed		PA (mm)	58,104	7807	20,547	16,380	8826	30	53,560	4336	90
		M (mm)	1937	260	685	546	294	1	1785	145	3
		SD (mm)	370	211	217	252	150	3	334	151	5
		CV (%)	19	81	32	46	51	285	19	104	171
		PTA (%)	100	13	35	28	15	0	92	7	0
BCC_CSM1.1	Raw data	PA (mm)	10,144	957	3504	2571	1107	50	8139	1161	676
		M (mm)	338	32	117	86	37	2	271	39	23
		SD (mm)	117	49	83	49	64	4	115	31	28
		CV (%)	35	153	71	57	173	243	42	80	122
		PTA (%)	100	9	35	25	11	0	80	11	7
	DBS corrected	PA (mm)	60,713	7244	22,466	19,559	8631	461	57,900	1435	820
		M (mm)	2024	241	749	652	288	15	1930	48	27
		SD (mm)	467	178	291	207	262	38	454	45	37
		CV (%)	23	74	39	32	91	248	24	94	135
		PTA (%)	100	12	37	32	14	1	95	2	1
CanESM1.1	Raw data	PA (mm)	17,987	1002	3425	5500	4627	457	14,554	1816	1019
		M (mm)	600	33	114	183	154	15	485	61	34
		SD (mm)	223	60	105	92	65	20	199	43	38
		CV (%)	37	180	92	50	42	133	41	71	112
		PTA (%)	100	6	19	31	26	3	81	10	6
	DBS corrected	PA (mm)	57,474	3759	12,734	19,722	18,191	498	54,406	1617	860
		M (mm)	1916	125	424	657	606	17	1814	54	29
		SD (mm)	709	177	356	308	238	34	693	64	41
		CV (%)	37	141	84	47	39	202	38	120	143
		PTA (%)	100	7	22	34	32	1	95	3	1
INM_CM4	Raw data	PA (mm)	23,418	544	4125	7302	4534	481	16,505	4209	2073
		M (mm)	781	18	138	243	151	16	550	140	69
		SD (mm)	202	19	95	83	64	9	129	95	54
		CV (%)	26	102	69	34	42	56	23	67	78
		PTA (%)	100	2	18	31	19	2	70	18	9
	DBS corrected	PA (mm)	65,362	1799	15,967	28,472	15,240	510	61,478	1868	1392
		M (mm)	2179	60	532	949	508	17	2049	62	46
		SD (mm)	633	90	408	441	239	50	606	86	48

Month/season			Annual	June	July	August	September	Pre-monsoon	Southwest monsoon	Post monsoon	Winter
		CV (%)	29	150	77	46	47	292	30	139	103
		PTA (%)	100	3	24	44	23	1	94	3	2
IPSL_CM5A_MR	Raw data	PA (mm)	23,491	482	2594	9134	6818	125	19,028	2848	1375
		M (mm)	783	16	86	304	227	4	634	95	46
		SD (mm)	281	19	72	175	86	7	243	67	39
		CV (%)	36	117	83	58	38	179	38	70	84
		PTA (%)	100	2	11	39	29	1	81	12	6
	DBS corrected	PA (mm)	70,983	2990	11,000	30,846	22,929	379	67,765	1355	1386
		M (mm)	2366	100	367	1028	764	13	2259	45	46
		SD (mm)	709	87	229	482	242	27	686	61	52
		CV (%)	30	87	62	47	32	214	30	135	113
		PTA (%)	100	4	15	43	32	1	95	2	2
NCAR_CCSM4	Raw data	PA (mm)	47,914	5290	13,795	13,365	8334	835	40,784	4608	1530
		M (mm)	1597	176	460	446	278	28	1359	154	51
		SD (mm)	254	140	150	150	119	26	254	59	37
		CV (%)	16	79	33	34	43	94	19	38	73
		PTA (%)	100	11	29	28	17	2	85	10	3
	DBS corrected	PA (mm)	58,001	6833	19,066	18,159	10,664	500	54,722	1841	827
		M (mm)	1933	228	636	605	355	17	1824	61	28
		SD (mm)	429	226	256	248	193	45	426	62	32
		CV (%)	22	99	40	41	54	269	23	101	115
		PTA (%)	100	12	33	31	18	1	94	3	1
NorESM1_M	Raw data	PA (mm)	31,286	1763	7389	10,970	6460	330	26,582	3143	1091
		M (mm)	1043	59	246	366	215	11	886	105	36
		SD (mm)	289	58	85	165	94	10	256	64	25
		CV (%)	28	99	34	45	44	90	29	61	68
		PTA (%)	100	6	24	35	21	1	85	10	3
	DBS corrected	PA (mm)	60,071	3171	15,558	24,862	13,522	439	57,113	1618	794
		M (mm)	2002	106	519	829	451	15	1904	54	26
		SD (mm)	687	141	216	434	231	30	658	65	33
		CV (%)	34	133	42	52	51	202	35	120	126
		PTA (%)	100	5	26	41	23	1	95	3	1
CERFACS_CNRM_CM5	Raw data	PA (mm)	21,830	2135	7702	7299	3149	77	20,285	1265	98
		M (mm)	728	71	257	243	105	3	676	42	3
		SD (mm)	161	49	78	91	79	4	156	49	6
		CV (%)	22	68	30	37	75	145	23	116	191

Month/season			Annual	June	July	August	September	Pre-monsoon	Southwest monsoon	Post monsoon	Winter
		PTA (%)	100	10	35	33	14	0	93	6	0
	DBS corrected	PA (mm)	58,535	5945	21,891	20,136	8001	482	55,973	1885	119
		M (mm)	1951	198	730	671	267	16	1866	63	4
		SD (mm)	450	149	227	270	207	37	438	100	9
		CV (%)	23	75	31	40	77	232	24	159	238
		PTA (%)	100	10	37	34	14	1	96	3	0
MPI_ESM_LR	Raw data	PA (mm)	14,291	1782	4080	3116	3502	103	12,480	1437	202
		M (mm)	476	59	136	104	117	3	416	48	7
		SD (mm)	116	45	61	53	80	17	118	45	16
		CV (%)	24	76	45	51	69	488	28	95	234
		PTA (%)	100	12	29	22	25	1	87	10	1
	DBS corrected	PA (mm)	66,279	9241	20,392	16,774	17,506	376	63,913	1684	230
		M (mm)	2209	308	680	559	584	13	2130	56	8
		SD (mm)	491	196	239	212	329	36	497	54	21
		CV (%)	22	63	35	38	56	288	23	97	267
		PTA (%)	100	14	31	25	26	1	96	3	0
HadGEM2_ES	Raw data	PA (mm)	4490	85	1191	1707	418	93	3401	701	203
		M (mm)	150	3	40	57	14	3	113	23	7
		SD (mm)	69	5	34	53	24	6	60	24	11
		CV (%)	46	185	86	92	172	200	53	104	166
		PTA (%)	100	2	27	38	9	2	76	16	5
	DBS corrected	PA (mm)	61,670	4892	22,051	24,714	7360	459	59,017	1792	321
		M (mm)	2056	163	735	824	245	15	1967	60	11
		SD (mm)	606	89	320	402	254	34	598	67	19
		CV (%)	29	55	44	49	103	225	30	113	174
		PTA (%)	100	8	36	40	12	1	96	3	1

Key: PA: precipitation accumulated; M: mean; SD (MM): standard deviation; CV: coefficient of variation and PTA: percentage to annual.

References

Annamalai, H., Hamilton, K., Sperber, K.R., 2007. The South Asian summer monsoon and its relationship with ENSO in the IPCC AR4 simulations. J. Clim. 20 (6), 1071–1092.

Ashley, R.M., Balmforth, D.J., Saul, A.J., Blanskby, J.D., 2005. Flooding in the future – predicting climate change, risks and responses in urban areas. Water Sci. Technol. 52 (5), 265–273.

Bergstrom, S., 2001. Climate change impacts on runoff in Sweden-assessments by Global Climate Models, dynamical downscaling and hydrological modelling. Clim. Res. 16 (2), 101.

Chen, H., Xu, C.-Y., Guo, S., 2012. Comparison and evaluation of multiple GCMs, statistical downscaling and hydrological models in the study of climate change impacts on runoff. J. Hydrol. 434–435, 36–45.

Dash, S.K., Kulkarni, M.A., Mohanty, U.C., Prasad, K., 2009. Changes in the characteristics of rain events in India. J. Geophys. Res.: Atmos. 114 (D10), D10109.

Fan, F., Mann, M.E., Lee, S., Evans, J.L., 2010. Observed and modeled changes in the South Asian summer monsoon over the historical period. J. Clim. 23 (19), 5193–5205.

Fowler, H.J., Blenkinsop, S., Tebaldi, C., 2007. Linking climate change modelling to impacts studies: recent advances in downscaling techniques for hydrological modelling. Int. J. Climatol. 27 (12), 1547–1578.

Gadgil, A., Dhorde, A., 2005. Temperature trends in twentieth century at Pune, India. Atmos. Environ. 39 (35), 6550–6556.

Giorgi, F., Jones, C., Asrar, G.R., 2009. Addressing climate information needs at the regional level: the CORDEX framework. WMO Bull. 58, 175–183.

Goswami, B.N., Venugopal, V., Sengupta, D., Madhusoodanan, M.S., Xavier, P.K., 2006. Increasing trend of extreme rain events over India in a warming environment. Science 314 (5804), 1442–1445.

Graham, L., Hagemann, S., Jaun, S., Beniston, M., 2007. On interpreting hydrological change from regional climate models. Clim. Change 81, 97–122.

Gupta, K., 2007. Urban flood resilience planning and management and lessons for the future: a case study of Mumbai, India. Urban Water J. 4 (3), 183–194.

Haylock, M.R., Peterson, T.C., Alves, L.M., Ambrizzi, T., Anunciacao, Y.M.T., Baez, J., Barros, V.R., Berlato, M.A., Bidegain, M., Coronel, G., Corradi, V., Garcia, V.J., Grimm, A.M., Karoly, D., Marengo, J.A., Marino, M.B., Moncunill, D.F., Nechet, D., Quintana, J., Rebello, E., Rusticucci, M., Santos, J.L., Trebejo, I., Vincent, L.A., 2006. Trends in total and extreme South American rainfall in 1960–2000 and links with sea surface temperature. J. Clim. 19 (8), 1490–1512.

Huntingford, C., Hugo Lambert, F., Gash, J.H.C., Taylor, C.M., Challinor, A.J., 2005. Aspects of climate change prediction relevant to crop productivity. Philos. Trans. R. Soc. B: Biol. Sci. 360 (1463), 1999–2009.

Huntington, T.G., 2006. Evidence for intensification of the global water cycle: review and synthesis. J. Hydrol. 319 (1–4), 83–95.

IPCC, 2007. Climate change, 2007: the physical science basis. In: Solomon, S., Qin, D., Manning, M., Chen, Z., Marquis, M., Averyt, K.B., Tignor, M., Miller, H.L. (Eds.), Contribution of Working Group I to the Fourth Assessment Report of the Intergovernmental Panel on Climate Change. Cambridge University Press, Cambridge, p. 996.

Kao, S.-C., Ganguly, A.R., 2011. Intensity, duration, and frequency of precipitation extremes under 21st-century warming scenarios. J. Geophys. Res. 116 (D16), D16119.

Kay, A.L., Reynard, N.S., Jones, R.G., 2006. RCM rainfall for UK flood frequency estimation. I. Method and validation. J. Hydrol. 318 (1–4), 151–162.

Kotlarski, S., 2005. Regional climate model simulations as input for hydrological applications: evaluation of uncertainties. Adv. Geosci. 5, 119.

Kripalani, R.H., Kulkarni, A., Sabade, S.S., Khandekar, M.L., 2003. Indian monsoon variability in a global warming scenario. Nat. Hazards 29 (2), 189–206.

Kripalani, R.H., Oh, J.H., Kulkarni, A., Sabade, S.S., Chaudhari, H.S., 2007. South Asian summer monsoon precipitation variability: coupled climate model simulations and projections under IPCC AR4. Theor. Appl. Climatol. 90 (3–4), 133–159.

Krishnan, R., Sabin, T.P., Ayantika, D.C., Kitoh, A., Sugi, M., Murakami, H., Turner, A.G., Slingo, J.M., Rajendran, K., 2013. Will the South Asian monsoon overturning circulation stabilize any further? Clim. Dyn. 40 (1–2), 187–211.

Kumar, K.K., Kamala, K., Rajagopalan, B., Hoerling, M.P., Eischeid, J.K., Patwardhan, S.K., Srinivasan, G., Goswami, B.N., Nemani, R., 2011. The once and future pulse of Indian monsoonal climate. Clim. Dyn. 36 (11–12), 2159–2170.

Kumke, T., 2001. Book Review: Regional Frequency Analysis: An Approach Based on L-Moments By J. R. M. Hosking and J. R. Wallis Cambridge University Press, Cambridge, UK, 1997, 224 p., $69.95 (U.S.), ISBN 0-521-43045-3 hardback. Mathematical Geology 33 (4), 535–537.

Lal, M., Meehl, G.A., Arblaster, J.M., 2000. Simulation of Indian summer monsoon rainfall and its intraseasonal variability in the NCAR climate system model. Reg. Environ. Change 1 (3–4), 163–179.

Lenderink, G., 2007. Estimates of future discharges of the river Rhine using two scenario methodologies: direct versus delta approach. Hydrol. Earth Syst. Sci. 11 (3), 1145.

Mailhot, A., Duchesne, S., Caya, D., Talbot, G., 2007. Assessment of future change in intensity-duration-frequency (IDF) curves for Southern Quebec using the Canadian Regional Climate Model (CRCM). J. Hydrol. 347 (1–2), 197–210.

Maraun, D., Wetterhall, F., Ireson, A.M., Chandler, R.E., Kendon, E.J., Widmann, M., Brienen, S., Rust, H.W., Sauter, T., Themeßl, M., Venema, V.K.C., Chun, K.P., Godess, C.M., Jones, R.G., Onof, C., Vrac, M., Eich, I.T., 2010. Precipitation downscaling under climate change: recent developments to bridge the gap between dynamical models and the end user. Rev. Geophys. 48 (3), RG3003.

May, W., 2002. Simulated changes of the Indian summer monsoon under enhanced greenhouse gas conditions in a global time-slice experiment. Geophys. Res. Lett. 29 (7), 22–31.

May, W., 2004. Simulation of the variability and extremes of daily rainfall during the Indian summer monsoon for present and future times in a global time-slice experiment. Clim. Dyn. 22 (2–3), 183–204.

May, W., 2011. The sensitivity of the Indian summer monsoon to a global warming of 2 °C with respect to pre-industrial times. Clim. Dyn. 37 (9–10), 1843–1868.

Meehl, G.A., Arblaster, J.M., 2003. Mechanisms for projected future changes in south Asian monsoon precipitation. Clim. Dyn. 21 (7–8), 659–675.

Min, S.-K., Zhang, X., Zwiers, F.W., Hegerl, G.C., 2011. Human contribution to more-intense precipitation extremes. Nature 470 (7334), 378–381.
Naidu, C.V., Rao, B.R.S., Rao, D.V.B., 1999. Climatic trends and periodicities of annual rainfall over India. Meteorol. Appl. 6 (4), 395–404.
Parthasarathy, B., Kumar, K.R., Munot, A.A., 1993. Homogeneous Indian monsoon rainfall – variability and prediction. Proc. Indian Acad. Sci. -Earth Planet. Sci. 102 (1), 121–155.
Pinto, J.G., Neuhaus, C.P., Leckebusch, G.C., Reyers, M., Kerschgens, M., 2010. Estimation of wind storm impacts over Western Germany under future climate conditions using a statistical–dynamical downscaling approach. Tellus A 62 (2), 188–201.
Ramesh Kumar, M.R., Krishnan, R., Sankar, S., Unnikrishnan, A.S., Pai, D.S., 2009. Increasing Trend of "Break-Monsoon" Conditions Over India—role of Ocean – atmosphere processes in the Indian Ocean. Geosci. Remote Sens. Lett., IEEE 6 (2), 332–336.
Rana, A., Bengtsson, L., Olsson, J., Jothiprakash, V., 2013. Development of IDF-curves for tropical india by random cascade modeling. Hydrol. Earth Syst. Sci. Discuss. 10 (4), 4709–4738.
Rana, A., Uvo, C., Bengtsson, L., Parth Sarthi, P., 2012. Trend analysis for rainfall in Delhi and Mumbai, India. Clim. Dyn. 38 (1), 45–56.
Ranger, N., Hallegatte, S., Bhattacharya, S., Bachu, M., Priya, S., Dhore, K., Rafique, F., Mathur, P., Naville, N., Henriet, F., Herweijer, C., Pohit, S., Morlot, J.C., 2011. An assessment of the potential impact of climate change on flood risk in Mumbai. Clim. Change 104 (1), 139–167.
Rupakumar, K., Sahai, A.K., Kumar, K.K., Patwardhan, S.K., Mishra, P.K., Revadekar, J.V., Kamala, K., Pant, G.B., 2006. High-resolution climate change scenarios for India for the 21st century. Curr. Sci. 90, 334–345.
Sabade, S.S., Kulkarni, A., Kripalani, R.H., 2011. Projected changes in South Asian summer monsoon by multi-model global warming experiments. Theor. Appl. Climatol. 103 (3–4), 543–565.
Schoof, J.T., Shin, D.W., Cocke, S., LaRow, E., Lim, Y.K., O'Brien, J.J., 2009. Dynamically and statistically downscaled seasonal temperature and precipitation hindcast ensembles for the southeastern USA. Int. J. Climatol. 29 (2), 243–257.
Semenov, V.S., Bengtsson, L.B., 2002. Secular trends in daily precipitation characteristics: greenhouse gas simulation with a coupled AOGCM. Clim. Dyn. 19 (2), 123–140.
Stainforth, D.A., Downing, T.E., Washington, R., Lopez, A., New, M., 2007. Issues in the interpretation of climate model ensembles to inform decisions. Philos. Trans. R. Soc. A: Math. Phys. Eng. Sci. 365 (1857), 2163–2177.
Stowasser, M., Annamalai, H., Hafner, J., 2009. Response of the South Asian summer monsoon to global warming: mean and synoptic systems. J. Clim. 22 (4), 1014–1036.
Teutschbein, C., Wetterhall, F., Seibert, J., 2011. Evaluation of different downscaling techniques for hydrological climate-change impact studies at the catchment scale. Clim. Dyn. 37 (9), 2087–2105.
Trenberth, K.E., 1999. Atmospheric moisture recycling: role of advection and local evaporation. J. Clim. 12 (5), 1368–1381.
Turner, A.G., Hannachi, A., 2010. Is there regime behavior in monsoon convection in the late 20th century? Geophys. Res. Lett. 37 (16), L16706.
Ueda, H., Iwai, A., Kuwako, K., Hori, M.E., 2006. Impact of anthropogenic forcing on the Asian summer monsoon as simulated by eight GCMs. Geophys. Res. Lett. 33 (6), L06703.
Van Vuuren, D.P., Edmonds, J., Kainuma, M., Riahi, K., Thomson, A., Hibbard, K., Hurtt, G.C., Kram, T., Krey, V., Lamarque, J.F., Masui, T., Meinshausen, M., Nakicenovic, N., Smith, S.J., Rose, S.K., 2011. The representative concentration pathways: an overview. Clim. Change 109, 5–31, http://dx.doi.org/10.1007/s10584-011-0148-z.
WCRP, 2011. Coupled Model Intercomparison Project – Phase 5, Special Issue of the CLIVAR Exchanges Newsletter, No. 56.
Wilby, R.L., Hay, L.E., Leavesley, G.H., 1999. A comparison of downscaled and raw GCM output: implications for climate change scenarios in the San Juan River basin, Colorado. J. Hydrol. 225 (1–2), 67–91.
Wilby, R.L., Wigley, T.M.L., 2002. Future changes in the distribution of daily precipitation totals across North America. Geophys. Res. Lett. 29 (7), 1135.
Willems, P., Arnbjerg-Nielsen, K., Olsson, J., Nguyen, V.T.V., 2012. Climate change impact assessment on urban rainfall extremes and urban drainage: methods and shortcomings. Atmos. Res. 103, 106–118.
Willems, P., Vrac, M., 2011. Statistical precipitation downscaling for small-scale hydrological impact investigations of climate change. J. Hydrol. 402 (3–4), 193–205.
Yang, W., Andreasson, J., Graham, L.P., Olsson, J., Rosberg, J., Wetterhall, F., 2010. Distribution-based Scaling to improve usability of regional climate model projections for hydrological climate change impacts studies. Hydrol. Res. 41 (3/4), 211–229.